# Direct Observation of Redox Induced Bubble Generation and Nanopore Formation Dynamics in Controlled Dielectric Breakdown

Ming Dong<sup>1</sup>, Zifan Tang<sup>1</sup>, Xiaodong He<sup>1</sup>, and Weihua Guan<sup>1,2\*</sup>

<sup>1</sup> Department of Electrical Engineering, Pennsylvania State University, University Park, Pennsylvania 16802, United States

<sup>2</sup> Department of Biomedical Engineering, Pennsylvania State University, University Park, Pennsylvania 16802, United States

\* Corresponding Author, Email: w.guan@psu.edu, Tel: 1-814-867-5748

## **ABSTRACT**

While controlled dielectric breakdown emerged as a promising method for accessible solidstate nanopore fabrication, there are still significant challenges in understanding the fabrication
dynamics due to the lack of *in-situ* cross-reference characterization beyond current monitoring. In
this work, we developed a multimodal method for characterizing the dielectric breakdown-based
nanopore formation dynamics. With this capability, we observed for the first time the redoxinduced bubble generation at the electrolyte-membrane interface. The randomly generated gas
bubble would significantly alter the electric field distribution on the membrane surfaces and is an
overlooked factor that can contribute to the random distribution of the nanopores. Besides, we
also studied the impact of electric field strength on the number and location of nanopore(s) initially
formed and after enlargement. We believe that the direct evidence of redox-induced bubble
formation and the impact of the electric field on nanopore formation dynamics presented in this
work would provide significant experimental insight for further improving the breakdown-based
solid-state nanopore fabrication.

## **KEYWORDS**

Solid-state nanopore, dielectric breakdown, multimodal characterization, redox, bubble

## Introduction

A solid-state nanopore is typically a nanometer-sized hole formed in a thin film membrane (usually  $SiN_x^{1,2}$  or  $SiO_2^3$ ). Due to its superior mechanical and chemical stability and the potential for integration into devices, a significant amount of research has been dedicated to this field, including new membrane materials<sup>4</sup>, fabrication techniques<sup>5, 6</sup>, and alternative sequencing<sup>7</sup>, sensing<sup>8</sup>, and diagnostic<sup>9</sup> strategies. The solid-state nanopore was usually fabricated by focused ion 10-12 or electron beams 13, 14. However, the cost and complexity of these instruments have created hurdles for researchers trying to access this promising sensor. To address this issue, an alternative controlled dielectric breakdown (CBD) method for nanopore fabrication was proposed<sup>15</sup> and further developed<sup>16-22</sup>. In this approach, a strong electric field causes a local material failure that leads to a nanoscale pinhole formation. The pioneering work by Kwok et al. 15 showed a nanopore down to 2 nm in size could be created by applying a constant voltage across the membrane until a time-dependent dielectric breakdown (TDDB) event occurs<sup>23, 24</sup>. The nanopore formation is signified by the measured membrane current reaching a predetermined cut-off level<sup>15, 17, 18</sup>. This method has been demonstrated to be useful for various materials, including silicon nitride (SiN<sub>x</sub>) as well as atomically thin two-dimensional materials such as graphene<sup>25, 26</sup>, and MoS<sub>2</sub><sup>27</sup>.

While the CBD method offers the potential for simplified and accessible nanopore fabrication, it is widely acknowledged that it suffers from the random distribution of numbers and locations of pores formed<sup>20, 28, 29</sup>. One obvious contributing factor for this randomness stems from the dielectric breakdown itself, a topic that has been studied in the field of microelectronics for decades<sup>30, 31</sup>. However, the CBD-based nanopore fabrication setup has a distinctive feature of involving both ionic and electronic transport in the system. The leakage current in the dielectric material such as SiN<sub>x</sub> should be carried by the electrons tunneling through randomly distributed defects in the

membrane<sup>15</sup>, while the current in the surrounding electrolyte should be carried by charged ions. For the current to go through the whole system, a redox reaction must occur at the electrolytemembrane interface. However, the impact of this redox reaction to the nanopore generation dynamics remains yet to be explored.

The stochastic nature of CBD-based nanopore fabrication critically calls for multimodal characterization *in-situ*. The typical CBD fabrication is often a black box experiment since the whole process is often only monitored by the current signal<sup>28, 32</sup>. However, a simple current measurement cannot distinguish between a single nanopore and multiple nanopores having the same total conductance. Although offline TEM-based imaging could provide significant detail about the nanopore size and shape, it is incredibly tedious to perform without knowing the rough location of the nanopore(s). Zrehen *et al.* adopted the wide-field fluorescence microscopy and calcium indicators for visualizing the number and the location of nanopores formed<sup>33</sup>. However, introducing the Ca<sup>2+</sup> chelator such as EGTA and indicator dye such as Fluo-4 may potentially lead to nanopore contamination that precludes further sensing experiments. It is preferred to characterize the formed nanopore in its native buffer conditions.

In this work, we developed a multimodal method for characterizing the nanopore formation dynamics in dielectric breakdown. With this capability, we directly observed for the first time the redox-induced bubble generation at the electrolyte-membrane interface. The randomly generated bubble would significantly alter the electric field distribution and is an overlooked factor that contributes to the random distribution of the nanopores. With this capability, we also studied the impact of electric field strength on the number and location of nanopore(s) initially formed and after enlargement. We believe that the direct evidence of redox-induced bubble formation and the impact of the electric field on nanopore formation dynamics presented in this work offers

significant experimental insight for nanopore breakdown fabrication.

## RESULTS AND DISCUSSION

### **Experimental Setup**

Figure 1a shows the schematic of the experimental setup with multiple capabilities (see methods for a detailed description). The SiN<sub>x</sub> membrane was assembled in a flow cell with cis and trans reservoirs filled with 1 M KCl buffered by Tris-EDTA. The flow cell was mounted onto and controlled by a nano-positioner. A collimated 488 nm laser was focused on the SiN<sub>x</sub> membrane. A pair of Ag/AgCl electrodes were placed in the reservoirs to apply the voltage bias and collect the current signal. The photoluminescence (PL) signal was collected by single photon counting modules (SPCM). The CMOS camera was used to monitor the microscopic environment changes during the fabrication process (e.g., redox-induced bubble generation). With this integrated setup, we could concurrently perform both the dielectric breakdown-based nanopore fabrication and multimodal characterization including monitoring in-situ, the conductance (IV),microenvironment variations (microscope), material variations (PL), and laser enhanced ionic current mapping for locating the nanopores<sup>34-37</sup>.

To validate the laser enhanced ionic current mapping in our setup for determining the nanopore numbers and locations, we used the TEM drilled nanopore samples as testing models. These TEM prepared samples have predefined numbers of the nanopore in known locations on the SiN<sub>x</sub> membrane. **Figure 1b&c** showed the results from representative samples containing a single nanopore and two nanopores, respectively. The nanopore location is annotated in the microscope images (left panel). The TEM characterizations of these nanopores were shown in the insets of the microscope images. For both samples, the corresponding PL (middle panel) and laser enhanced

ionic current mapping results (right panel) both showed distinguishable features in the nanopore location. It is noteworthy that the PL reduction in SiN<sub>x</sub> is very sensitive to the electronic structure change and does not necessarily indicate the location of a physical nanopore<sup>38, 39</sup>. In this work, we mostly used the laser enhanced ionic current mapping for determining the nanopore numbers and locations, while the complementary PL result was only used for reference. It is also worth mentioning that while increasing the laser power can help to improve the signal to noise ratios in laser-induced ionic current enhancement (**Supporting Figure S1**), high laser power is detrimental to the material integrity of SiN<sub>x</sub> membrane<sup>5, 39, 40</sup>. In this work, we used 6 mW laser for the laser enhanced ionic current mapping, unless otherwise noted.

#### Breakdown and in-situ Characterization

We previously reported a moving Z-score based breakdown method<sup>28</sup> for nanopore fabrication. Briefly, each abnormal current jump event (defined by a moving Z-score > 6) during the high voltage stressing is cross-verified by repetitive IV characterizations at low voltages. A physical formation of nanopores in the membrane (true positive) would require all IV measurements to have conductance larger than 1 nS and coefficient of determination (R<sup>2</sup>) higher than 0.85. While this method significantly reduced false positives, the conductance measurement alone lacks the capability to determine the nanopore locations and numbers. With the multimodal characterization setup shown in **Figure 1**, we were able to address this issue.

Figure 2 shows a representative breakdown fabrication and *in-situ* characterization process. First, the pristine  $SiN_x$  membrane was examined by IV characterization between  $\pm 0.1V$  (top row), laser enhanced ionic current mapping (middle row), and microscope (bottom row). Second, a bias of 12 V was applied and the current trace as well as the moving Z-score values were recorded in

real-time. Once an abnormal event was detected, the 12 V bias was removed immediately. A cross-verify process was then performed. As shown in the third column in **Figure 2**, both IV and laser enhanced ionic current mapping confirmed there was no physical nanopore formation. As a result, a second trial under 12 V bias was performed (fourth column in **Figure 2**) until another abnormal event was detected. The subsequent cross-verify process (fifth column in **Figure 2**) showed that physical breakdown indeed occurred (conductance and R<sup>2</sup> values fall into the shaded area), and there was a single nanopore in the SiN<sub>x</sub> membrane (confirmed by laser enhanced ionic current mapping). In this case, since we now have confirmation that a single nanopore was formed, its diameter could be estimated as 3.1 nm using  $G = \sigma \left(\frac{4h}{\pi D^2} + \frac{1}{D}\right)^{-1}$ , in which  $\sigma$ , h, and D represent the electrolyte conductivity, membrane thickness and the nanopore diameter, respectively<sup>41</sup>. Another representative case involving more rounds of breakdown trials can be found in **Supporting Figure S2**. These results showed that the multimodal characterization could provide the much-needed information about the nanopore location and number for interpreting the conductance results.

#### **Direct Observation of Redox Induced Bubble Generation**

Surprisingly, we observed the bubble formation around the SiN<sub>x</sub> membrane during the breakdown trial when the membrane was subject to high voltage stress. As shown in the microscope image in the second column of **Figure 2**, a gas bubble (annotated by an arrow) was clearly visible under 12 V bias. It is noteworthy that the bubble formation is universal for all the 15 samples we tested (**Supporting Figure S3**). As shown in the second column in **Figure 2**, the ionic current was not obviously affected by the bubble generation, and this may because the

initially formed bubble covered only a small region of the  $SiN_x$  membrane. This intriguing bubble formation phenomenon in nanopore breakdown fabrication was directly observed for the first time. **Supporting Video S1** aggregates the bubble formation dynamics in 8 of these 15 samples. These bubbles showed random morphology and spatial distribution on the  $SiN_x$  membrane. Moreover, these bubbles do not necessarily disappear after the biasing voltage was removed. These randomly generated bubbles by redox reactions would significantly alter the electric field distribution. The bubbles could also prevent further redox reactions at the bubble covered locations, which prevents nanopore formation at that location since fewer charges can be transferred to the areas beneath the bubble. As shown in **Figure 2** and **Supporting Figure S3**, the locations of bubbles were different from the locations of nanopores. The bubble generation during the breakdown is thus a previously overlooked factor that can contribute to the random location of the nanopores.

To understand this phenomenon, we hypothesized that a redox reaction must occur at the electrolyte-membrane interface such that the ionic transport in the electrolyte and the electronic transport in the SiN<sub>x</sub> membrane can continuously flow throughout the system. Since a typical breakdown voltage in the order of 10 V and the standard electrochemical potential for KCl and H<sub>2</sub>O at 25 °C and pH 8 is 1.396 V and 1.228 V, respectively, we hypothesized that the bubbles formed during the breakdown fabrication are most likely due to the following redox reactions at the interface (**Figure 3**). The oxidation of chloride ions at the interface generates chlorine gas  $(2 Cl^- \rightarrow Cl_2(g) + 2 e^-)$  and provides electrons. These electrons travel through the SiN<sub>x</sub> membrane via trap-assisted tunneling<sup>15</sup>. When they arrived at the other interface of the membrane, these electrons contributed to the generation of H<sub>2</sub> gas by the reduction of hydrogen ions  $(2 H^+ + 2 e^- \rightarrow H_2(g))$ . Interestingly, Briggs *et al.* previously found that the time-to-pore formation was significantly reduced when the positively biased reservoir is filled with a highly acidic solution.<sup>29</sup>

This observation is in excellent agreement with our hypothesized redox process. When reducing the pH value, the available hydrogen ions for the reduction reaction is increased. This would help increase the rate of electron transfer at the lower interface (**Figure 3**) and increase the rate of defect formation. As a result, shorter time-to-pore could be expected when adding acidic solutions<sup>29</sup>. Besides, the traps formed by possible hydrogen ions penetration into membrane could promote trap-assisted tunneling, and thus shorten the time-to-pore<sup>30</sup>. In principle, a higher bubble generation rate would be expected if increasing the concentration of the species participated in redox reactions. However, based on the random morphology of the bubbles observed, the nucleation and evolution of bubbles on the SiN<sub>x</sub> membrane is indeed complex, and it is challenging to precisely quantify the bubble number and size.

## **Explore the Impact of Breakdown Electric Field on Nanopore Locations and Numbers**

With the multimodal characterization setup, we explored the impact of the breakdown electric field on nanopore locations and numbers. A total of nine samples were fabricated by the moving Z-score method<sup>28</sup> under three different voltages. **Figure 4a** showed the laser enhanced ionic current mapping of formed nanopores after the initial breakdown, from which we were able to determine the formed nanopore locations and numbers for each sample. **Figure 4b** showed the initially formed nanopore numbers as a function of the breakdown electric field. For all three samples fabricated at 0.8 V/nm, only a single nanopore was observed. When the breakdown electric field increased to 1.0 V/nm, we started to see one of the samples showed three pores after the breakdown. In the case of 1.2 V/nm, the initial breakdown can lead to as many as five pores. While a larger sample size would be required to establish meaningful statistics, it is generally observed that a low electric field should be preferred to avoid forming multiple pores<sup>2, 20, 33</sup>. This is intuitively reasonable since the high electric field can generate defects faster, thus increasing the

possibility of producing multiple nanopores<sup>32, 33</sup>. We also examined the locations of the formed nanopores in all samples we tested. As shown in **Figure 4c**, the spatial distribution of initially formed nanopores showed no tendency to a specific area and can be regarded as random. While this is expected due to the stochastic nature of the dielectric breakdown<sup>15</sup>, we believe the redoxinduced bubble formation before the breakdown occurring is another factor that contributed to the location randomness (**Supporting Video S1**).

## **Explore the Nanopore Enlargement Dynamics**

The initially formed nanopore was often enlarged to a specific size by an electric field to meet the requirement for different analytes, or to get a more stabilized ionic current signal 15, 20, 21, <sup>42</sup>. It was hypothesized that extra nanopores might form during the enlargement process<sup>20, 33</sup>. However, direct evidence of this hypothesis is limited. With the capacity to determine the nanopore locations and numbers in our multimodal setup, we were able to observe the nanopore enlargement dynamics directly. For each of the initially fabricated samples containing a single nanopore, we performed the sequential enlargement process at three different electric fields (0.2, 0.4 and 0.6 V/nm). After each enlargement process, laser enhanced ionic current mapping was performed to determine if extra nanopores were formed (Figure 5a). Figure 5b shows the extra nanopore numbers as a function of the enlargement electric field. No extra nanopore was formed for all seven samples enlarged under 0.2 V/nm (first row in Figure 5a). When increasing the enlargement electric field to 0.4 V/nm (second row in Figure 5a), 2 out of 7 samples (#5 and #8) showed extra pores were formed after enlargement. When the enlargement electric field was increased further to 0.6 V/nm (third row in Figure 5a), 5 out of 7 samples showed extra pores. As can be clearly seen from Figure 5b, enlargement at higher electric field indeed increased the chance to form extra

pores instead of enlarging the existing single nanopore<sup>20</sup>. The results shown in **Figure 5b** suggested that a low electric field was favorable for the enlargement process if the single nanopore is desirable. Nevertheless, due to the experimental and material variations, the possibility of forming additional pores during the enlargement process cannot be simply ruled out.

## **CONCLUSION**

In summary, we developed a multimodal method for *in-situ* characterizing the nanopore formation dynamics in dielectric breakdown. With the capability of monitoring microscopic environment changes during the fabrication process, we directly observed for the first time the redox-induced bubble generation at the electrolyte-membrane interface. The randomly generated bubble is an overlooked factor that contributes to the random location of the nanopores since the electric field distribution could be significantly altered. The impact of the electric field on CBD nanopore locations and numbers was also explored. For the initially formed pores, their spatial distribution is random, which stems not only from the stochastic nature of the SiN<sub>x</sub> membrane breakdown, but also from the redox-induced bubbles at the interface. In addition, multiple nanopores can be simultaneously formed at high breakdown electric fields due to fast defect generation. Further, the formation of extra pores during the electric-field based enlargement of a single pore was verified by our setup. It was found that a low electric field is favorable for forming single nanopore during initial formation and enlargement. These findings offered critical experimental insight for performing breakdown-based solid-state nanopore fabrication.

#### **METHODS**

Materials and Chemicals. 15 nm thick SiN<sub>x</sub> membranes were used in our experiments (Norcada, Canada). The square membrane with a 50 × 50 μm<sup>2</sup> window is at the center of a 200 μm thick silicon frame. Samples with TEM (JEOL JEM-2100F, operated at 200 kV) drilled nanopore(s) were provided by our collaborator. The SiN<sub>x</sub> membranes were mounted into PMMA based flow cell with Ecoflex-5 (Smooth-On). Ag/AgCl electrodes were house made with 0.375 mm Ag wires (Warner Instruments, Hamden, USA). Potassium chloride and 1X EDTA Tris buffer solution (pH 8.0) were purchased from Sigma-Aldrich. The solution was filtered with a 0.2 μm Anotop filter (Whatman) and degassed in a vacuum chamber prior to use.

**Instrumentation.** The SiN<sub>x</sub> membrane was mounted into a flow cell with a transparent quartz coverslip bottom. The cis and trans chambers were filled with 1 M KCl in 1X EDTA Tris buffer. The flow cell was mounted on a nano-positioner (Physik Instrumente, P-611.3S NanoCube). The Keithley 2636 was used to apply voltage bias and collect current signals through Ag/AgCl electrodes. The 488 nm laser (Coherent OBIS 488 LS) was firstly expanded to completely fill the back aperture before focusing at the SiN<sub>x</sub> membrane through the microscope objective lens (magnification 40×, numerical aperture 0.75) to form a diffraction-limited spot for confocal illumination. The laser spot radius is around 1.2 µm. The emitted light was collected by the same objective lens and focused on a pinhole with 25 µm diameter (1-25+B-1+M-0.5, National Aperture) for improved spatial resolution. The emission light was filtered by a bandpass filter before detected by the single photon counting module (SPCM-AQRH-13). A neutral-density (ND) filter was mounted in the front of the photon counter to expand the dynamic range. A CMOS camera (DCC1545M, Thorlabs) was also equipped for monitoring the microscopic environment changes during the fabrication process. The whole setup was shielded by a Faraday cage to minimize electromagnetic interferences.

Nanopore Fabrication and Characterization. The moving Z-score method was adopted for the

nanopore fabrication, and details about this method can be found in our previous work<sup>28</sup>. The

abnormal events were checked by IV characterization between  $\pm 0.1V$  and laser enhanced ionic

current mapping. With a customized LabVIEW program (National Instruments) that controls the

motion of nano-positioner and thus the laser irradiation region, the laser enhanced ionic current

mapping could be performed to collect the current intensity distribution of the whole membrane.

The typical mapping parameters in our experiments are 500 nm step size, 6 mW laser power,

200mV voltage bias, and 2 ms integration time.

ASSOCIATED CONTENT

The Supporting Information is available.

SNR relationship with different mapping laser power, another sample's fabrication process,

CMOS camera snapshots of bubbles.

**AUTHOR INFORMATION** 

**Corresponding Author** 

\* Email: w.guan@psu.edu

**ORCID** 

Weihua Guan: 0000-0002-8435-9672

**Author contributions** 

D.M. designed and carried out the nanopore fabrication and characterization experiment. D.M.,

T.Z., and H.X. built the optical setup. W.G. conceived the concept and supervised the study. W.G.

13

and D.M. co-wrote the manuscript, discussed it with all other authors.

## **NOTES**

The authors declare no competing financial interest.

## **ACKNOWLEDGMENTS**

This work supported by the National Science Foundation under Grant No. 1710831, 1902503, and 1912410. Any opinions, findings, and conclusions or recommendations expressed in this work are those of the authors and do not necessarily reflect the views of the National Science Foundation. W.G. acknowledges the support from Penn State Startup Fund.

## FIGURES AND CAPTIONS

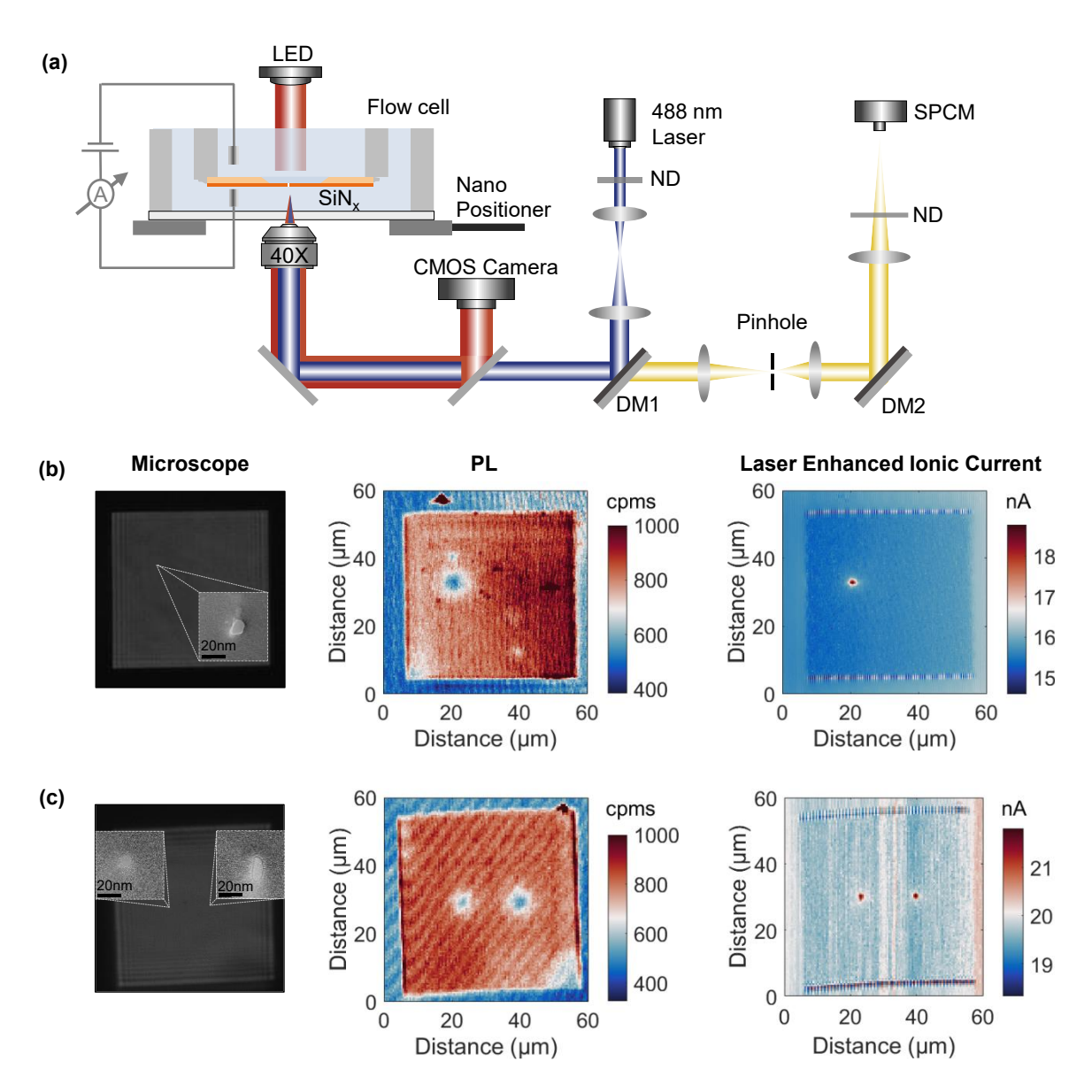
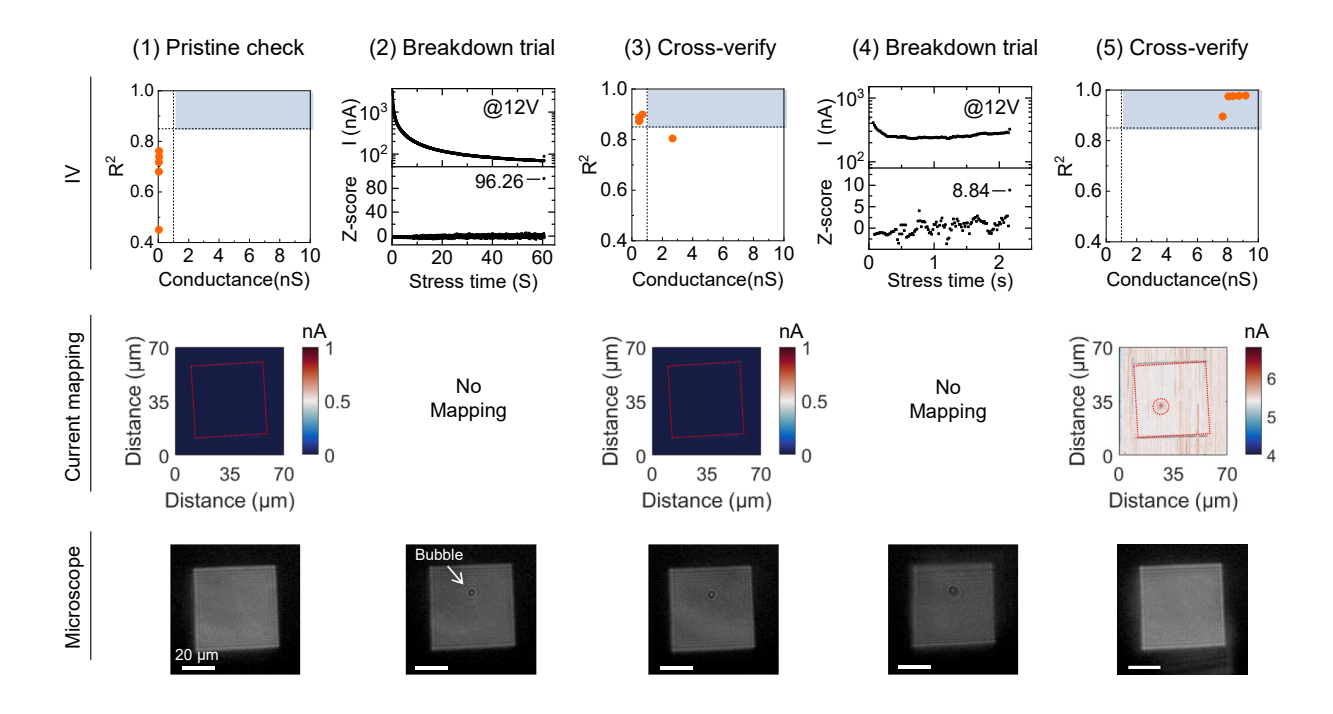
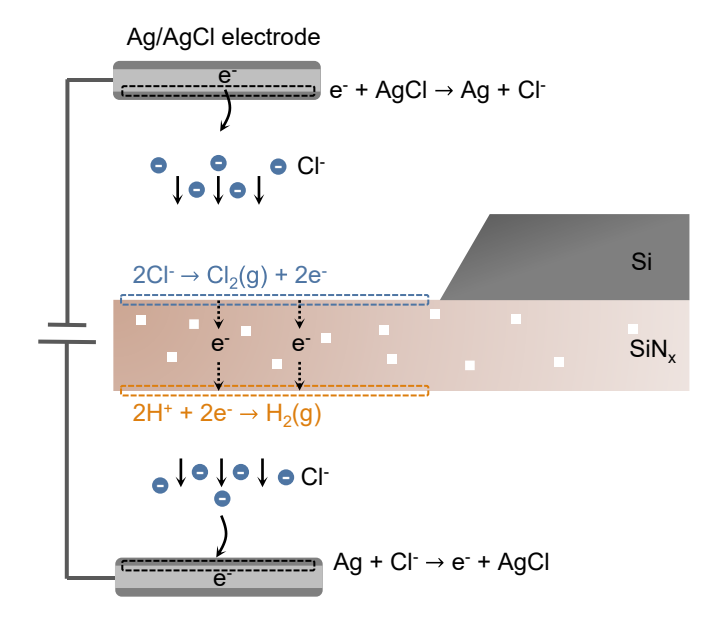


Figure 1. (a) Schematic of the setup for breakdown-based nanopore fabrication and multimodal characterization (DM: dichroic mirror, ND: neutral-density filter). (b) The result from TEM drilled model samples containing a single nanopore. (c) The result from TEM drilled model samples containing two nanopores. In (b) and (c), Left panel: microscope image showing the location of the nanopore on the SiN<sub>x</sub> membrane (inset: TEM image of the nanopore); Middle panel: PL result obtained under 2 mW laser and 2 ms integration time; Right panel: laser enhanced ionic current obtained under 6 mW and 200 mV mapping laser voltage bias.



**Figure 2**. Multimodal characterization of nanopores formation dynamics in the fabrication process. The first row is IV characterization (between  $\pm 0.1$ V), current and Z-score traces for nanopore formation monitoring. The second row is laser enhanced ionic current mapping obtained under 200 mV voltage and 6 mW. The third row is the microscopic image of the membrane.



**Figure 3**. Schematic of ionic transport in the electrolyte and the electronic transport in the SiNx membrane. The reduction reaction at Ag/AgCl cathode generates chloride ions, and these ions move towards the top surface of the SiNx membrane by electrophoresis. The oxidation of chloride ions at the interface will generate chlorine gas and provide electrons. The electrons could travel through the SiNx membrane via trap-assisted tunneling (White squares indicate the traps). When electrons arrive at the other interface, they can contribute to the generation of hydrogen gas by the reduction of hydrogen ions.

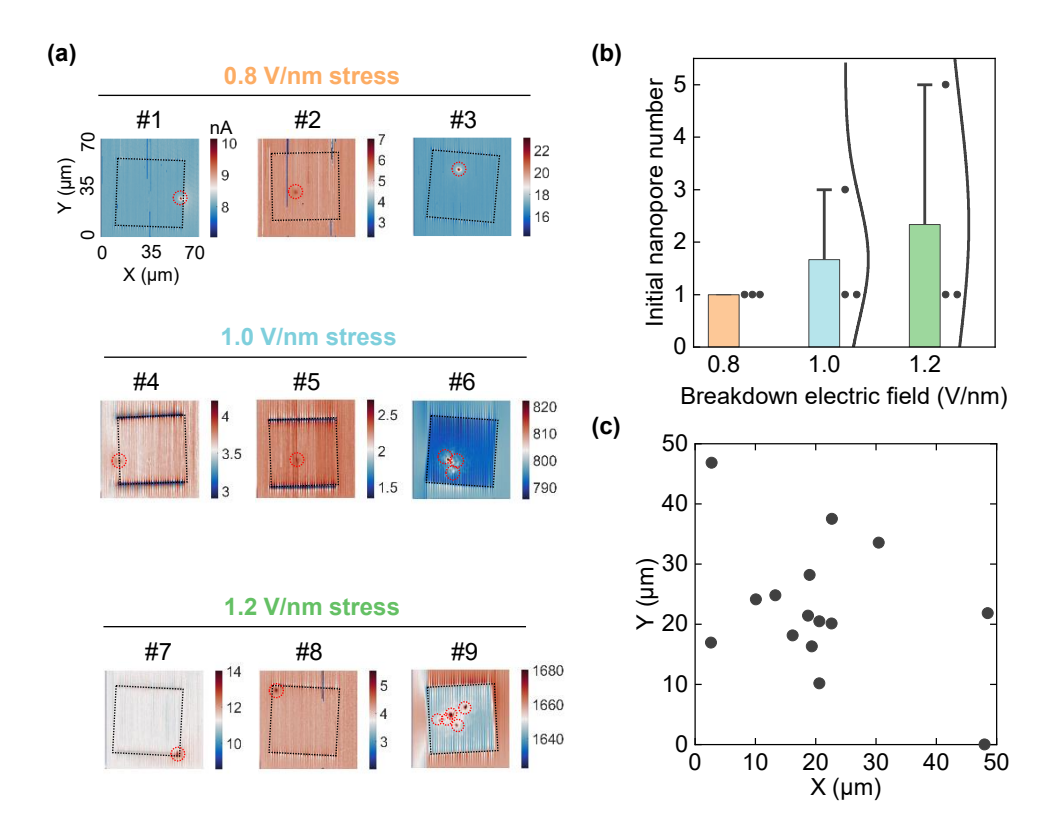


**Figure 4**. (a) Laser enhanced ionic current mapping for 9 samples breakdown by different electric fields. The thickness of  $SiN_x$  membranes is 15 nm. (b) The number distribution of initially formed nanopores at different breakdown electric fields. (c) The spatial distribution of the initially formed nanopores.

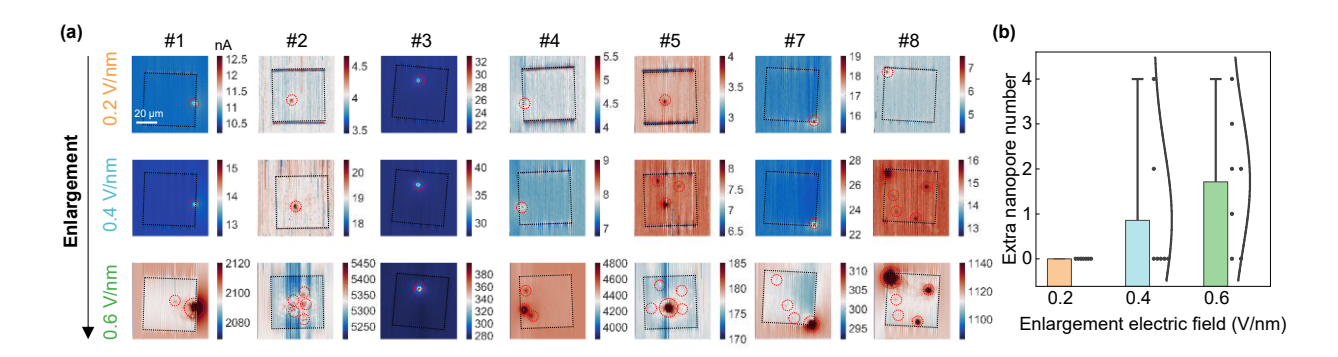


**Figure 5**. (a) Laser enhanced ionic current mapping of 7 samples containing single nanopore sequentially enlarged at three different electric fields. First enlargement with 0.2 V/nm for 30s, second enlargement with 0.4 V/nm for 30s and third enlargement with 0.6 V/nm for 2s. (b) The number distribution of extra pores formed after each enlargement process.

#### REFERENCES

- 1. Chen, P.; Mitsui, T.; Farmer, D. B.; Golovchenko, J.; Gordon, R. G.; Branton, D., Atomic layer deposition to fine-tune the surface properties and diameters of fabricated nanopores. *Nano Letters* **2004**, *4* (7), 1333-1337.
- 2. Ying, C.; Houghtaling, J.; Eggenberger, O. M.; Guha, A.; Nirmalraj, P.; Awasthi, S.; Tian, J.; Mayer, M., Formation of Single Nanopores with Diameters of 20–50 nm in Silicon Nitride Membranes Using Laser-Assisted Controlled Breakdown. *ACS Nano* **2018**, *12* (11), 11458-11470.
- 3. Danelon, C.; Santschi, C.; Brugger, J.; Vogel, H., Fabrication and functionalization of nanochannels by electron-beam-induced silicon oxide deposition. *Langmuir* **2006**, *22* (25), 10711-10715.
- 4. Wilson, J.; Sloman, L.; He, Z.; Aksimentiev, A., Graphene nanopores for protein sequencing. *Advanced Functional Materials* **2016**, *26* (27), 4830-4838.
- 5. Gilboa, T.; Zrehen, A.; Girsault, A.; Meller, A., Optically-monitored nanopore fabrication using a focused laser beam. *Scientific Reports* **2018**, *8*, 9765.
- 6. Zhang, Y.; Miyahara, Y.; Derriche, N.; Yang, W.; Yazda, K.; Capaldi, X.; Liu, Z.; Grutter, P.; Reisner, W., Nanopore Formation via Tip Controlled Local Breakdown Using an Atomic Force Microscope. *Small Methods* **2019**, *3* (7), 1900147.
- 7. Jain, M.; Koren, S.; Miga, K. H.; Quick, J.; Rand, A. C.; Sasani, T. A.; Tyson, J. R.; Beggs, A. D.; Dilthey, A. T.; Fiddes, I. T., Nanopore sequencing and assembly of a human genome with ultra-long reads. *Nature Biotechnology* **2018**, *36* (4), 338-345.
- 8. Shi, W.; Friedman, A. K.; Baker, L. A., Nanopore sensing. *Analytical Chemistry* **2017**, *89* (1), 157-188.
- 9. Charalampous, T.; Kay, G. L.; Richardson, H.; Aydin, A.; Baldan, R.; Jeanes, C.; Rae, D.; Grundy, S.; Turner, D. J.; Wain, J., Nanopore metagenomics enables rapid clinical diagnosis of bacterial lower respiratory infection. *Nature Biotechnology* **2019**, *37* (7), 783-792.
- 10. dela Torre, R.; Larkin, J.; Singer, A.; Meller, A., Fabrication and characterization of solid-state nanopore arrays for high-throughput DNA sequencing. *Nanotechnology* **2012**, *23* (38), 385308.
- 11. Schiedt, B.; Auvray, L.; Bacri, L.; Oukhaled, G.; Madouri, A.; Bourhis, E.; Patriarche, G.; Pelta, J.; Jede, R.; Gierak, J., Direct FIB fabrication and integration of "single nanopore devices" for the manipulation of macromolecules. *Microelectron Eng* **2010**, *87* (5-8), 1300-1303.
- 12. Li, J.; Stein, D.; McMullan, C.; Branton, D.; Aziz, M. J.; Golovchenko, J. A., Ion-beam sculpting at nanometre length scales. *Nature* **2001**, *412* (6843), 166-169.
- 13. Lin, T. C.; Wang, Y. C.; Wang, Z.; Wang, S. Y.; Wang, D. C., A Straight Nanopore Drilling by Transmission Electron Microscope. *Applied Mechanics and Materials* **2013**, *395-396*, 179-183.
- 14. Storm, A. J.; Chen, J. H.; Ling, X. S.; Zandbergen, H. W.; Dekker, C., Fabrication of solid-state nanopores with single-nanometre precision. *Nature Materials* **2003**, *2* (8), 537-540.
- 15. Kwok, H.; Briggs, K.; Tabard-Cossa, V., Nanopore Fabrication by Controlled Dielectric Breakdown. *Plos One* **2014**, *9* (3), e92880.
- 16. Bello, J.; Mowla, M.; Troise, N.; Soyring, J.; Borgesi, J.; Shim, J., Increased dwell time and occurrence of dsDNA translocation events through solid state nanopores by LiCl concentration gradients. *Electrophoresis* **2019**, *40* (7), 1082-1090.

- 17. Briggs, K.; Kwok, H.; Tabard-Cossa, V., Automated Fabrication of 2-nm Solid-State Nanopores for Nucleic Acid Analysis. *Small* **2014**, *10* (10), 2077-2086.
- 18. Kwok, H.; Waugh, M.; Bustamante, J.; Briggs, K.; Tabard-Cossa, V., Long Passage Times of Short ssDNA Molecules through Metallized Nanopores Fabricated by Controlled Breakdown. *Advanced Functional Materials* **2014**, *24* (48), 7745-7753.
- 19. Wang, Y.; Chen, Q.; Deng, T.; Liu, Z., Self-Aligned Nanopore Formed on a SiO2 Pyramidal Membrane by a Multipulse Dielectric Breakdown Method. *The Journal of Physical Chemistry C* **2018**, *122* (21), 11516-11523.
- 20. Wang, Y.; Ying, C.; Zhou, W.; de Vreede, L.; Liu, Z.; Tian, J., Fabrication of multiple nanopores in a SiN x membrane via controlled breakdown. *Scientific Reports* **2018**, *8*, 1234.
- 21. Yanagi, I.; Hamamura, H.; Akahori, R.; Takeda, K.-i., Two-step breakdown of a SiN membrane for nanopore fabrication: Formation of thin portion and penetration. *Scientific Reports* **2018**, *8*, 10129.
- 22. Yanagi, I.; Akahori, R.; Hatano, T.; Takeda, K., Fabricating nanopores with diameters of sub-1 nm to 3 nm using multilevel pulse-voltage injection. *Scientific Reports* **2014**, *4*, 5000.
- 23. Hirayama, M.; Asai, S.; Matsumoto, H.; Sawada, K.; Nagasawa, K., Time-Dependent Dielectric-Breakdown of Thin Sio2-Films. *Jpn J Appl Phys* **1981**, *20* (5), L329-L332.
- 24. McPherson, J. W., Time dependent dielectric breakdown physics Models revisited. *Microelectron Reliab* **2012**, *52* (9-10), 1753-1760.
- 25. Kuan, A. T.; Lu, B.; Xie, P.; Szalay, T.; Golovchenko, J. A., Electrical pulse fabrication of graphene nanopores in electrolyte solution. *Appl Phys Lett* **2015**, *106* (20), 203109.
- 26. Wang, L. D.; Boutilier, M. S. H.; Kidambi, P. R.; Jang, D.; Hadjiconstantinou, N. G.; Karnik, R., Fundamental transport mechanisms, fabrication and potential applications of nanoporous atomically thin membranes. *Nature Nanotechnology* **2017**, *12* (6), 509-522.
- 27. Feng, J.; Liu, K.; Graf, M.; Lihter, M.; Bulushev, R. D.; Dumcenco, D.; Alexander, D. T. L.; Krasnozhon, D.; Vuletic, T.; Kis, A.; Radenovic, A., Electrochemical Reaction in Single Layer MoS2: Nanopores Opened Atom by Atom. *Nano Letters* **2015**, *15* (5), 3431-3438.
- 28. Roshan, K. A.; Tang, Z.; Guan, W., High fidelity moving Z-score based controlled breakdown fabrication of solid-state nanopore. *Nanotechnology* **2019**, *30* (9), 095502.
- 29. Briggs, K.; Charron, M.; Kwok, H.; Le, T.; Chahal, S.; Bustamante, J.; Waugh, M.; Tabard-Cossa, V., Kinetics of nanopore fabrication during controlled breakdown of dielectric membranes in solution. *Nanotechnology* **2015**, *26* (8), 084004.
- 30. DiMaria, D.; Cartier, E.; Arnold, D., Impact ionization, trap creation, degradation, and breakdown in silicon dioxide films on silicon. *Journal of Applied Physics* **1993**, *73* (7), 3367-3384.
- 31. Puurunen, R. L., Surface chemistry of atomic layer deposition: A case study for the trimethylaluminum/water process. *Journal of Applied Physics* **2005**, *97* (12), 9.
- 32. Carlsen, A. T.; Briggs, K.; Hall, A. R.; Tabard-Cossa, V., Solid-state nanopore localization by controlled breakdown of selectively thinned membranes. *Nanotechnology* **2017**, *28* (8), 085304.
- 33. Zrehen, A.; Gilboa, T.; Meller, A., Real-time visualization and sub-diffraction limit localization of nanometer-scale pore formation by dielectric breakdown. *Nanoscale* **2017**, *9* (42), 16437-16445.
- 34. Yamazaki, H.; Hu, R.; Henley, R. Y.; Halman, J.; Afonin, K. A.; Yu, D.; Zhao, Q.; Wanunu, M., Label-free single-molecule thermoscopy using a laser-heated nanopore. *Nano Letters* **2017**, *17* (11), 7067-7074.

- 35. Di Fiori, N.; Squires, A.; Bar, D.; Gilboa, T.; Moustakas, T. D.; Meller, A., Optoelectronic control of surface charge and translocation dynamics in solid-state nanopores. *Nature Nanotechnology* **2013**, *8* (12), 946-951.
- 36. Tsuji, T.; Sasai, Y.; Kawano, S., Thermophoretic manipulation of micro-and nanoparticle flow through a sudden contraction in a microchannel with near-infrared laser irradiation. *Physical Review Applied* **2018**, *10* (4), 044005.
- 37. Danda, G.; Drndić, M., Two-dimensional nanopores and nanoporous membranes for ion and molecule transport. *Current Opinion in Biotechnology* **2019**, *55*, 124-133.
- 38. Assad, O. N.; Di Fiori, N.; Squires, A. H.; Meller, A., Two color DNA barcode detection in photoluminescence suppressed silicon nitride nanopores. *Nano Letters* **2014**, *15* (1), 745-752.
- 39. He, X.; Tang, Z.; Liang, S.; Liu, M.; Guan, W., Confocal scanning photoluminescence for mapping electron and photon beam induced microscopic changes in SiNx during nanopore fabrication. *Nanotechnology* **2020**, *31*, 395202.
- 40. Yamazaki, H.; Hu, R.; Zhao, Q.; Wanunu, M., Photothermally assisted thinning of silicon nitride membranes for ultrathin asymmetric nanopores. *ACS Nano* **2018**, *12* (12), 12472-12481.
- 41. Kowalczyk, S. W.; Grosberg, A. Y.; Rabin, Y.; Dekker, C., Modeling the conductance and DNA blockade of solid-state nanopores. *Nanotechnology* **2011**, *22* (31), 315101.
- 42. Beamish, E.; Kwok, H.; Tabard-Cossa, V.; Godin, M., Precise control of the size and noise of solid-state nanopores using high electric fields. *Nanotechnology* **2012**, *23* (40), 405301.

# For TOC only

